# A numerical study on the elastic modulus of volume and area dilation for a deformable cell in a microchannel

Ji Young Moon,[1,2] Roger I. Tanner,[2] and Joon Sang Lee[1,a)]
[1]*School of Mechanical Engineering, Yonsei University, Seoul, South Korea*
[2]*School of Aerospace, Mechanical and Mechatronic Engineering, The University of Sydney, Sydney, New South Wales 2006, Australia*

(Received 5 May 2016; accepted 21 July 2016; published online 4 August 2016)

A red blood cell (RBC) in a microfluidic channel is highly interesting for scientists in various fields of research on biological systems. This system has been studied extensively by empirical, analytical, and numerical methods. Nonetheless, research of predicting the behavior of an RBC in a microchannel is still an interesting area. The complications arise from deformation of an RBC and interactions among the surrounding fluid, wall, and RBCs. In this study, a pressure-driven RBC in a microchannel was simulated with a three-dimensional lattice Boltzmann method of an immersed boundary. First, the effect of boundary thickness on the interaction between the wall and cell was analyzed by measuring the time of passage through the narrow channel. Second, the effect of volume conservation stiffness was studied. Finally, the effect of global area stiffness was analyzed. *Published by AIP Publishing.* [http://dx.doi.org/10.1063/1.4960205]

## INTRODUCTION

Understanding the deformation of a cell is important to predict its properties in a microchannel, path selection in a blood vessel, and metastasis of cancer cells.[1–3] In the past, to measure cell properties, a single cell had to be extracted by means of devices such as a micropipette, optical tweezer, or atomic force microscopy (AFM).[4–6] The development of recent microfluidic methods led to various protocols for quantification of cell properties in a microchannel without extracting stand-alone cells.[7,8] Few of those methods include straining the cell with filters at the outlet of the channel, measurement of the time for the cells to reach the outlet, and separation of cells by density, size, or deformability.[9,10] These methods enable us to measure averaged properties of a cell, but it is not available to measure amounts of force on a single cell.[11] To overcome these limitations of experiments and to uncover the hidden physics behind various phenomena, computational fluid dynamics (CFD) is used lately.[3,12–15]

Most of the studies by CFD solve the solid and fluid separately in different grids and then analyze the interaction between them by an interpolation method. The deformation and migration of the solid are calculated by assuming the no-slip boundary condition at the solid-fluid interface. These deformations and migration of the solid are then applied to the fluid as an external force. The fluid itself is solved by several methods such as Navier-Stokes equations, dissipative particle dynamics, or the lattice Boltzmann method (LBM).[16–19] These solutions for the fluid are well known and suitable for general use, but the solution for the solid is not simple. To solve the solid, the stretching and bending of the membrane must be analyzed at least.[17] Moreover, many studies stipulate the equilibrium of volume and surface for solid models.[12,16,19–22] There are also various models to solve the viscoelasticity of the cell.[18,23,24]

[a)]E-mail: joonlee@yonsei.ac.kr. Tel.: +82 2-2123-5820.

The numerical approach of the cell deformation has received considerable attention in numerous areas such as membrane property, fluctuation of membranes, and multi scale modeling of cells to hydrodynamic interaction techniques. Generally, the deformation of cells is expressed in network membrane that uses triangular membranes. Various studies have been done to apply the complicated property of a cell in the triangular membranes.[14,22,32] In order to describe the complicated properties of cell, shear and bending elasticity, area stretching, and volume conservation should be analyzed and the parameters for each of these properties are needed to be determined. These parameters are derived by empirical data.[5] In order to apply empirical data in the simulation, the constants that determine the cell property are derived by calibration. A few researchers have provided a rigidity value of the cell in the simulation as a deformation variable;[16] however, it is difficult to use it without calibration unless the numerical method, computational domain, and timescale in the simulation are exactly the same.

Other researchers described the relation among shear modulus, area dilation, and bending coefficients. They interpreted the cell properties by using equations of shear modulus, enabling it to describe the cell by means of a single shear modulus.[12,25] Furthermore, a few researchers explained the volume constraint coefficient that is chosen large enough to restrain initial volume.[16] Similarly, there have been attempts to solve global area dilation, where the explanation of equation derivation is also large enough to approximate the membrane. Therefore, it is difficult to apply the empirical cell properties to a simulation directly without calibration. Studies of cell deformation to the changes in values of each constant representing the cell properties are required for cell simulation and for prediction of the cell's characteristic based on the cell's behavior.

The objectives of this paper are to conduct a parametric study to analyze the volume stiffness $K_V$ and global area dilation stiffness $K_{AG}$ of four parameters and to determine the relation between them and the cell deformation. Many researchers examined the deformation and migration of cells inside a fluid with ideal shear flow,[26,27] but this method is relatively difficult for setting up an experiment. In contrast, our study is performed under microchannel conditions. For the cell, the biconcave shape of a red blood cell (RBC) is used.

The influence of $K_V$ and $K_{AG}$ in a global simulation as well as the cell deformation and migration as a function of boundary thickness are being examined here. The time for cells to pass through the channel is measured at different values of $K_V$ and $K_{AG}$, along with the analysis of the degree of deformation and transit time. Moreover, the velocity and deformation of cells as a function of boundary thickness are also studied. LBM is used for the fluid solution, whereas the immersed boundary methods are applied to fluid structure interactions. The numerical methods for solving cell deformation and migration inside a microchannel are explained in detail in this paper.

## NUMERICAL METHODS

### Lattice Boltzmann method

This method is widely used to solve microfluidics.[3,28–30] The single-relaxation-time Bhatnagar-Gross-Krook model is used to solve an incompressible fluid. The governing equation with the forcing term can be written as[31]

$$f_i(\mathbf{x}+\mathbf{e}_i\Delta t, t+\Delta t) - f_i(\mathbf{x},t) = -\frac{1}{\tau}\left(f_i(\mathbf{x},t) - f_i^{eq}(\mathbf{x},t)\right) + \Delta t\left(1-\frac{1}{2\tau}\right)\omega_i\left[\frac{\mathbf{e}_i-\mathbf{u}}{{c_s}^2} + \frac{(\mathbf{e}_i\cdot\mathbf{u})}{{c_s}^4}\mathbf{e}_i\right]\cdot\mathbf{f}, \tag{1}$$

with the local equilibrium distribution function

$$f_i^{eq} = \rho\omega_i\left[1 + \frac{1}{{c_s}^2}\mathbf{e}_i\cdot\mathbf{u} + \frac{1}{2{c_s}^4}(\mathbf{e}_i\cdot\mathbf{u})^2 - \frac{1}{2{c_s}^2}\mathbf{u}\cdot\mathbf{u}\right], \tag{2}$$

where for the D3Q19 model

$$\omega_i \begin{cases} \frac{1}{3}, & i = 0 \\ \frac{1}{18}, & i = 1, 2, ..., 6 \\ \frac{1}{36}, & i = 7, 8, ..., 18 \end{cases} \tag{3}$$

$$e_i \begin{cases} (0,0,0) & i = 0 \\ (\pm 1,0,0), (0,\pm 1,0), (0,0,\pm 1) & i = 1, 2, ..., 6 \\ (\pm 1,\pm 1,0), (\pm 1,0,\pm 1), (0,\pm 1,\pm 1) & i = 7, 8, ..., 18. \end{cases} \tag{4}$$

In the above equation, the density distribution function $f_i(\mathbf{x}, t)$ indicates the proportion of particles moving with the $i$ th lattice velocity at lattice site x and time $t$, $\Delta t$ is the time step, $\tau$ is the particle relaxation time, $\mathbf{e}_i$ is the discrete microscopic velocity, $f_i^{eq}$ is the local equilibrium distribution function, and $c_s (= c/\sqrt{3})$ is the speed of sound ($c = \Delta \mathbf{x}/\Delta t$). Fluid density $\rho$ and velocity $\mathbf{u}$ can be calculated using the following formula:

$$\rho = \sum_i f_i \quad \rho \mathrm{u} = \sum_i f_i \mathrm{e}_i. \tag{5}$$

The kinematic viscosity is given as

$$\nu = \left(\tau - \frac{1}{2}\right) {c_s}^2 \Delta t. \tag{6}$$

Please refer to the Appendix for the detailed conversion of LBM units to *Systeme International* (SI) units.

### 3D deformable particle mechanics

To understand RBC deformation, the fluid-structure interactions among the membrane of RBCs, internal fluid of RBCs, and plasma need to be considered. The spring network models have been used to solve deformation of biological cells such as RBCs and other deformable particles such as hydrocapsules.[3,12,17] The triangular meshes, which are the most common meshes for the spectrin network of RBC membranes, were used. For the constrained spontaneous shape of RBCs, volume, area, stretching, and bending were solved.[16,20,32,33] A viscoelastic spring network model, which takes into account the total volume conservation, surface area dilation, bending, and stretching of the membrane as well as mesh density, was used.[16,32]

The membrane of RBC is represented by the spring network consisting of Lagrangian nodes shown in Fig. 1. The stretching force between Lagrangian nodes $X_1$ and $X_2$ can be written as

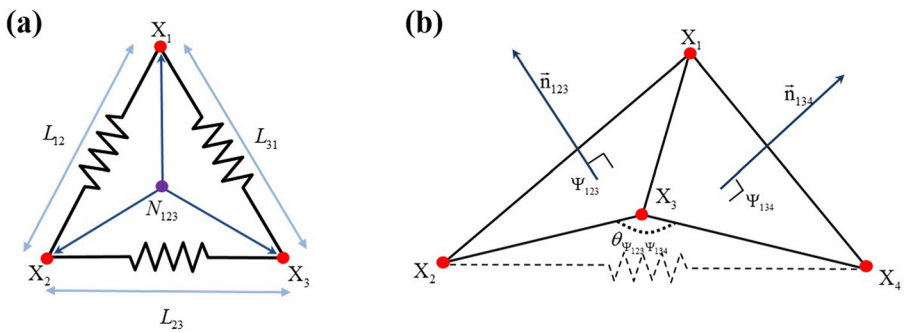


FIG. 1. The spring network of faces $\Psi_{123}$ and $\Psi_{134}$. (a) $L$ is the distance between Lagrangian nodes. $N_{123}$ is the center of three nodes: $X_1$, $X_2$, and $X_3$. (b) $\vec{n}$ is the normal vector of face $\Psi$, $\theta_{\Psi_{123}\Psi_{134}}$ is the instantaneous angle between two faces: $\Psi_{123}$ and $\Psi_{134}$.

$$\mathrm{F}^S(\mathrm{X}_1,\mathrm{X}_2) = -\mathrm{F}^S(\mathrm{X}_2,\mathrm{X}_1) = -k_S\kappa(\lambda_{12})\Delta L_{12}\vec{L}_{12} \quad (\Delta L_{12} = L_{12} - L^0{}_{12}), \tag{7}$$

where $k_S$ is the stretching constant. The non-linear (hyperelastic) function for neo-Hookean behaviour $\kappa$ is found as[26]

$$\kappa(\lambda_{12}) = \frac{(\lambda_{12})^{0.5} + (\lambda_{12})^{-2.5}}{\lambda_{12} + (\lambda_{12})^{-3}}, \quad \left(\lambda_{12} = \frac{L_{12}}{L^0_{12}}\right), \tag{8}$$

where $L$ is the instantaneous distance and $L_0$ is the spontaneous distance between Lagrangian nodes.

The normal vector of face $\Psi_{123}$ can be written as

$$\vec{\mathrm{n}}_{123} = (\mathrm{X}_2 - \mathrm{X}_1) \times (\mathrm{X}_3 - \mathrm{X}_1)/|(\mathrm{X}_2 - \mathrm{X}_1) \times (\mathrm{X}_3 - \mathrm{X}_1)|. \tag{9}$$

The center of the plane is expressed as

$$N_{123} = \frac{(\mathrm{X}_1 + \mathrm{X}_2 + \mathrm{X}_3)}{3}. \tag{10}$$

The bending force between faces $\Psi_{123}$ and $\Psi_{134}$ can be formulated as

$$\mathrm{F}^B(\mathrm{X}_2)/\vec{\mathrm{n}}_{123} = \mathrm{F}^B(\mathrm{X}_4)/\vec{\mathrm{n}}_{134} = -k_B[1 - \cos(\theta_{\Psi_{123}\Psi_{134}} - \theta^0{}_{\Psi_{123}\Psi_{134}})], \tag{11}$$

$$\theta_{\Psi_{123}\Psi_{134}} = \pi - \cos^{-1}(\vec{\mathrm{n}}_{123} \cdot \vec{\mathrm{n}}_{123}) \ \textit{when}\ c_{\Psi_{123}\Psi_{134}} \le 0$$
$$\textit{otherwise}\ \theta_{\Psi_{123}\Psi_{134}} = \pi + \cos^{-1}(\vec{\mathrm{n}}_{123} \cdot \vec{\mathrm{n}}_{123}), \tag{12}$$

$$c_{\Psi_{123}\Psi_{134}} = (N_{123} - N_{134}) \cdot \vec{\mathrm{n}}_{123}, \tag{13}$$

$$\mathrm{F}^B(\mathrm{X}_3) = \mathrm{F}^B(\mathrm{X}_3) = \frac{\mathrm{F}^B(\mathrm{X}_2) + \mathrm{F}^B(\mathrm{X}_4)}{2}, \tag{14}$$

where $k_B$ is the bending constant, $\theta$ is the instantaneous angle, and $\theta_0$ is the spontaneous angle, respectively. $c_{\Psi\Psi}$ is the angle indicator that determines whether the angle is obtuse or acute.

The spring energy system to solve the deformation relates a one-triangle face to the overall energy can be written as[12,33,35,36]

$$E^{AL}(\Psi_{123}) = k_{AL}\frac{(\Delta A(\Psi_{123}))^2}{2A(\Psi_{123})}. \tag{15}$$

Similarly, the volume energy can also be expressed as[20]

$$E^V(\Psi_{1231}) = -k_V\frac{(V - V_0)^2}{V_0}\vec{\mathrm{n}}_{123}. \tag{16}$$

The spring network model in this paper is a simplified alternative model instead of energy model. The area and volume conservation constraints can be obtained as[21,32]

$$\mathrm{F}^A(\Psi_{123},\mathrm{X}_1) = \mathrm{F}^{AL}(\Psi_{123},\mathrm{X}_1) + \mathrm{F}^{AG}(\Psi_{123},\mathrm{X}_1) = -\left(k_{AL}\frac{\Delta A(\Psi_{123})}{\sqrt{A(\Psi_{123})}} + k_{AG}\frac{\Delta A_T}{A_T}\right)(\mathrm{X}_1 - N_{123}), \tag{17}$$

$$A(\Psi_{123}) = ((\mathrm{X}_2 - \mathrm{X}_1) \times (\mathrm{X}_3 - \mathrm{X}_1))/2, \tag{18}$$

$$\mathrm{F}^V(\Psi_{123},\mathrm{X}_1) = -k_V\frac{V - V_0}{3V_0}A(\Psi_{123})\vec{\mathrm{n}}_{123}, \tag{19}$$

$$V = \sum_{\Psi} (N \cdot \vec{n}) A(\Psi)/3, \tag{20}$$

where $k_{AL}$, $k_{AG}$, and $k_V$ are the local area, global area, and volume constraint constants, respectively. The terms $A_T$, $V$, and $V_0$ are the total area, instantaneous total volume, and spontaneous total volume, respectively.

Total elastic force under the constrained spontaneous shape can be formulated as

$$\mathrm{F} = \mathrm{F}^V + \mathrm{F}^A + \mathrm{F}^S + \mathrm{F}^B. \tag{21}$$

### Lattice Boltzmann immersed boundary method

The immersed boundary method for the interaction between the fluid and RBC is as follows:[37–39]

$$\mathbf{f}(\mathbf{x}, t) = \int D(\mathbf{x} - \mathbf{X}(\mathbf{s}, t)) \mathbf{F}(\mathbf{s}, t) d\mathbf{s}, \tag{22}$$

$$\frac{\partial \mathbf{X}(\mathbf{s}, t)}{\partial t} = \mathbf{u}(\mathbf{X}(\mathbf{s}, t), t) = \int \mathbf{u}(\mathbf{x}, t) D(\mathbf{x} - \mathbf{X}(\mathbf{s}, t)) d\mathbf{x}, \tag{23}$$

$$D(\mathbf{x} - \mathbf{X}(\mathbf{s}, t)) = \frac{1}{64h^3} \left(1 + \cos\left(\frac{\pi x}{2h}\right)\right) \left(1 + \cos\left(\frac{\pi y}{2h}\right)\right) \left(1 + \cos\left(\frac{\pi z}{2h}\right)\right)_{for\ D3Q19}$$
$$when\ |x\ and\ y\ and\ z| \leq 2h,\ otherwise\ D(\mathbf{x}) = 0, \tag{24}$$

where $\mathbf{f}$, $\mathbf{x}$, and $\mathbf{u}$ are the force density acting on the fluid node, Eulerian coordinates, and fluid velocity, respectively. $\mathbf{X}$ and $\mathbf{F}$ are the Lagrangian coordinates and restoring force density of the RBC, respectively. $D$ is the Dirac delta function for interpolation. Equations (22)–(24) represent the immersed boundary equation for communication between Eulerian and Lagrangian coordinates. Unknown factors are the force per unit volume, $\mathbf{f}(\mathbf{x}, t)$, applied by the immersed boundary to the fluid, and the velocity of each Lagrangian node $\mathbf{u}(\mathbf{X}(\mathbf{s}, t), t)$. Equation (22) describes the force density of fluid, $\mathbf{f}(\mathbf{x}, t)$, calculated from Lagrangian restoration of the elastic force density, $\mathbf{F}(\mathbf{s}, t)$, via interpolation over the immersed boundary. Equation (23) assumes that the no-slip boundary condition is applied to the membrane because the Lagrangian nodes move at the same velocity as the surrounding fluid. Equation (24) uses the 3D Dirac delta function, $\mathbf{D}(\mathbf{x} - \mathbf{X}(\mathbf{s}, t))$, which relates interactions between Eulerian coordinates (fluid nodes) and Lagrangian coordinates (deformable particle boundary nodes).

## RESULTS

### Simulation overview

Figure 2 shows a schematic of the domain used for simulation of a red blood cell (RBC) in a microchannel. The formula of Evans and Fung[40] is used to describe the geometry of the RBC

$$T(r) = \sqrt{1 - (r/R_0)^2} [C_0 + C_1 (r/R_0)^2 + C_2 (r/R_0)^4]. \tag{25}$$

T(r) is the thickness of RBC and is determined by the location of the radius of the RBC toward its center. The following parameters are used: $R_0 = 3.9\mu$m, $C_0 = 0.81\mu$m, $C_1 = 7.83\mu$m, $C_2 = -4.39\mu$m, $T_1 = 0.81\mu$m, and $T_2 = 2.4\mu$m. Our analysis of geometric features of the microchannel is inspired by resent empirical results[11,41,42] and simulation results.[12,13] The length of the domain is $L = 24\mu$m, height of the domain is $H = 4.8\mu$m, width of domain is $w = 3.2\mu$m, the length of the wide segment is $l_1 = 8\mu$m, length of the narrow segment is $l_2 = 4\mu$m, and the connected angle between the narrow segment and width is $\theta = 45^\circ$.

The body force is added at all fluid nodes to set the pressure gradient driven flow. The pressure gradient can be expressed as a function of $L$

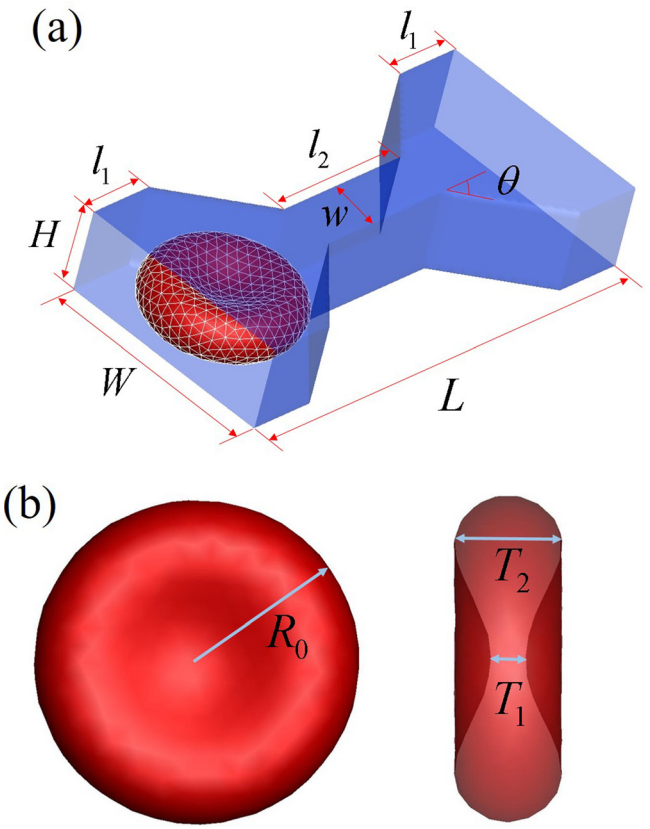


FIG. 2. (a) A schematic of the domain used for simulation of a red blood cell (RBC) in a microchannel. $L$ is the length of the domain, $H$ is the height of the domain, $W$ is the width of the domain, $l_1$ is the length of the wide segment, $l_2$ is the length of the narrow segment, $w$ is the width of the narrow section, and $\theta$ is the connected angle between the narrow segment and width. (b) The shape of the RBC is described by Eq. (25).

$$\Delta P = \rho L F^P. \tag{26}$$

For all cases in this study, one pressure gradient as 12Pa is used. The characteristic velocity and time in this simulation can be calculated: $U = \Delta P w^2/(8\mu L)$ and $T = L/U$, respectively. Capillary number $Ca$ represents the relative effect of viscous and elastic forces and is defined as follows:

$$Ca = \mu U/G_s. \tag{27}$$

$Ca$ values in this study are used in the range 0.011 to 0.055.

Physiologically, an RBC is composed of a membrane and inner fluid. The inner fluid is called the cytosol, which contains hemoglobin and other proteins. The membrane of RBC encloses a viscous of cytosol.[33] Because of these components, the cytosol has greater viscosity than plasma does. The viscosity difference between plasma and cytosol affects the cell deformation and motion. In this study, the cytosol viscosity and plasma viscosity are set $\mu = 10^{-3}$ Pa s to reduce the viscosity difference effect and for simplicity, as in many other numerical studies.[12,17,33] The density values of the RBC and plasma are set to $\rho = 1000\,\mathrm{kg/m^3}$.

The stretching constant $k_S$ and area dilation constant $k_{AL}$ for most of the deformable solid simulations are based on a continuum model, which is determined by shear modulus $G_s = \frac{\sqrt{3}}{4}k_S$ and Young's modulus $E = \frac{2}{\sqrt{3}}k_S$.[34] It is hard to change three values $k_S$, $k_{AL}$, $k_B$ separately for a certain property. For the sake of simplicity and generalization, the dimensionality of the constant value of elasticity is reduced as using the ratio between the bending forces and in-plane stretching forces. The ratio of a bending force to stretching force can be estimated as $\xi = k_B/(R^2 k_S) = O(10^{-3})$.[12,25] Similarly, dilation modulus can be estimated as $k_A/k_S = 2.0$.

For the wall-cell interaction, a repulsive force is added. This force is needed to avoid boundary penetration, as commonly done in the field of fluid structure interactions.[12,43] As the repulsive force, the cutoff spring model is used, which can be expressed as

$$\mathrm{F}^W = \begin{cases} 0 & \delta_d > \delta_r \\ -k_w \delta_d & \delta_d \le \delta_r \end{cases}, \tag{28}$$

where $\delta_d$ is the instantaneous distance between the cell and wall and $\delta_r$ is the boundary thickness of the gap to activate the repulsive force, respectively.

The repulsive stiffness $k_W$ is set to a value four to seven orders of magnitude greater than the shear modulus.[43] $k_W = 0.1$ is used for the repulsive stiffness.

Wu and Feng[12] used root mean square deviation of the displacement ratio with instantaneous distance $L$ and spontaneous distance to obtain the local deformation $\varepsilon$ on the cell membrane. The local deformation can be formulated as

$$\varepsilon = \sqrt{\frac{\sum \left(\frac{L}{L_0} - 1\right)^2}{N_S}}, \tag{29}$$

where $N_S$ is the number of spring connections at each node. This approach is very effective at determining deformation on the cell membrane quantitatively. The local deformation contour is used to show the deformation on the cell membrane.

## Validation

One of the most general methods for validation of numerical results on a deformable cell is a comparison with the optical tweezer experiment.[5] For this procedure, the numerical experiment of optical tweezer was set with the following values for healthy human RBCs: $k_S = 0.00126$, $k_{AL} = 0.002$, $k_B = 0.00029$, $k_V = 0.008$, $k_{AG} = 0.02$. The axial and transverse diameters of the RBCs were measured at different stretching forces. These results were compared with optical tweezer experiment results[5] and other numerical simulation results.[17] Axial and transverse diameters were defined as the longest distance in each direction. Figure 3 shows the comparison among our results, empirical data, and other numerical results.

The simulation of the trajectories of RBCs through the narrow channel for three values are shown in Fig. 4 for the comparison with the data of Wu and Feng.[12] The transit time of both results has increased by the increase of $G_s$ from 5 to 15 $\mu$N/m. Both results have shown that RBC could not pass through the channel when $G_s = 25\,\mu$N/m. The cause of the difference

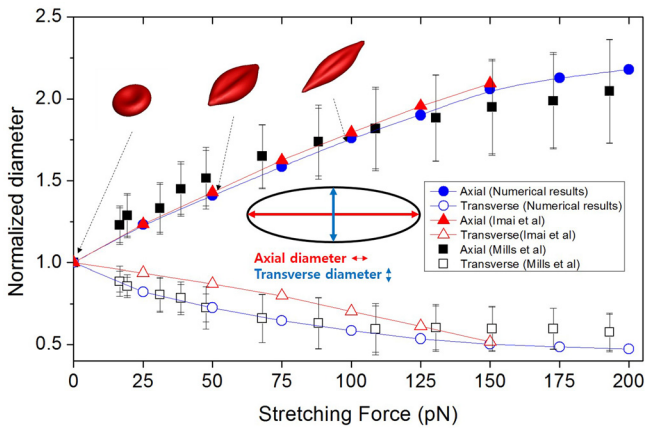


FIG. 3. Comparison among optical tweezer experiment results,[5] other numerical simulation data,[15] and numerical results in this paper.

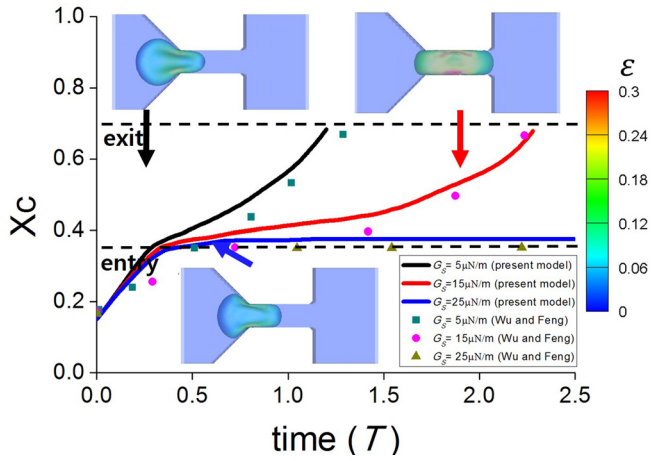


FIG. 4. Trajectories of red blood cells (RBCs) through the narrow channel as function of the characteristic time for three values.

between two results is from the difference of RBC model and boundary conditions applied in the simulation. The tendency between two results is matched with each other. The cause of the difference between two results is from the difference of RBC model and boundary conditions applied in the simulation.

### Effects of boundary thickness of the gap

A full description of the microchannel with a deformable cell requires a complete understanding of the interactions between cells, between the cells and the fluid, between the wall and the fluid, and between the cell and the wall. In this subsection, the interaction between the cell and wall is focused on as boundary thickness changes.

Figure 5 shows the trajectories of an RBC through the narrow channel at different values of boundary thickness. The properties of the RBC in both cases were set to be the same $G_s = 5\ \mu\text{N/m}$ ($k_S = 0.001, k_{AL} = 0.002, k_B = 0.00029$), $k_V = 0.008, k_{AG} = 0.01$. The only difference among the three cases was boundary thickness, which was $\delta_r = 1.0$, $\delta_r = 1.5$, and $\delta_r = 2.0$, respectively. In Fig. 4(d), the vertical axis of graph $X_c/L$ represents the instantaneous position of the center of mass for a flow direction, which is normalized to the length of the domain, and the horizontal axis

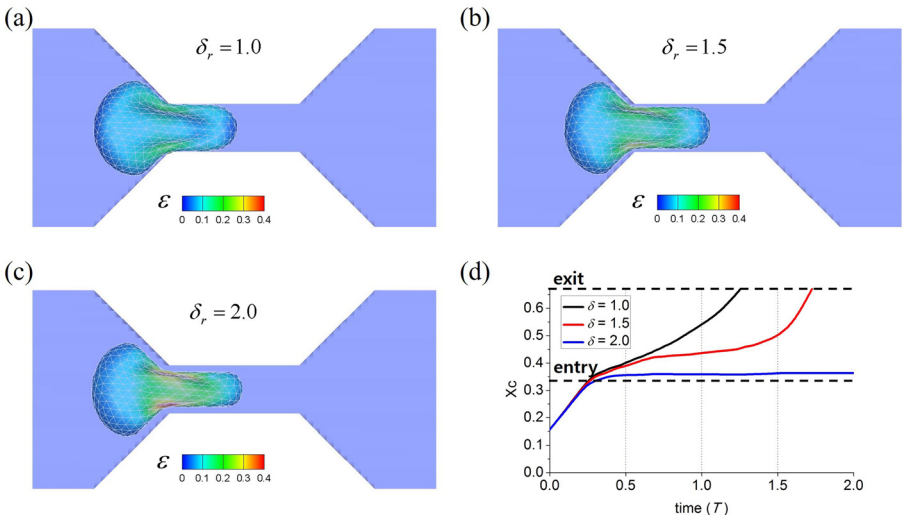


FIG. 5. Trajectories of red blood cells (RBCs) through a narrow channel at $T = 0.35$ for different values of boundary thickness: (a) $\delta_r = 1.0$, (b) $\delta_r = 1.5$, and (c) $\delta_r = 2.0$. (d) Normalized location of the center of mass $X_c/L$ plotted against characteristic time for the simulation. The membrane shear modulus $G_s = 5\ \mu\text{N/m}$ for the three cases.

of the graph represents the characteristic time in the simulation. The entry of the channel was defined as a starting point of a narrow channel and the exit of the channel as an ending point of a narrow channel. Figures 5(a)–5(c) illustrate a snapshot of the RBC shapes at $T = 0.26$. The fluid layer between the RBC and the wall becomes thicker as $\delta_r$ increases; the increase of $\delta_r$ leads to more deformation in the narrow channel. In this case, as the size of the gap increases, the actual area where the RBC can exist decreases, thus behaving as if the width of the channel itself is decreased. Figure 5(d) shows that the increase in boundary thickness decreases the RBC velocity. This result can be seen as a numerical error because general microfluidics explains that the boundary thickness between an RBC and channel wall increases as the capillary number increases.[35] To solve this problem, the boundary thickness should be small enough. While the boundary thickness is too small ($\delta_r < 1$), the repulsive force might be changed dramatically and cause the unnatural deformation of RBC. All subsequent results are presented at $\delta_r = 1.0$.

### Effects of volume stiffness $k_V$

The value $k_V$ is necessary to maintain the cell as incompressible in the simulation. When volume of the cell decreases at high $k_V$, the pressure inside the cell increases to maintain the original volume. $k_V$ is related to permeability of the cell.[44] To apply the shear modulus change for area dilation constant, the weight factor of shear modulus $f(G_s)$ is used: $G_s = 5, 15, 25(\mu\text{N/M}) \rightarrow f(G_s) = 1, 3, 5$.

Figure 6 shows a comparison of four cases to examine the relation between $k_V$ and deformation, along with three types of shear modulus. Stiffness of each parameter is shown in Table I. When shear modulus is low, then an increase in $k_V$ increases transit time of the RBC in the channel. The transit time is defined as the period between the time point when the center of mass of the RBC reaches the entry and the time point when it reaches the exit.

According to Fig. 6(a), when $k_V$ is 0, the change in RBC movement under the influence of shear modulus is small. Moreover, when $k_V$ is 0, the RBC cannot restore its original shape after passing through the narrow channel. As $k_V$ increases, the duration of RBC's stay in the narrow channel also increases, and when shear modulus is 25 $\mu$N/m and $k_V = 0.011$, the RBC cannot pass through the channel. Even though $k_V$ is not a constant for the membrane elasticity, this behavior of the RBC is similar to that of a malaria-infected RBC in the microchannel. When the RBC is infected with malaria, the merozoites remodel the spectrin network; this change

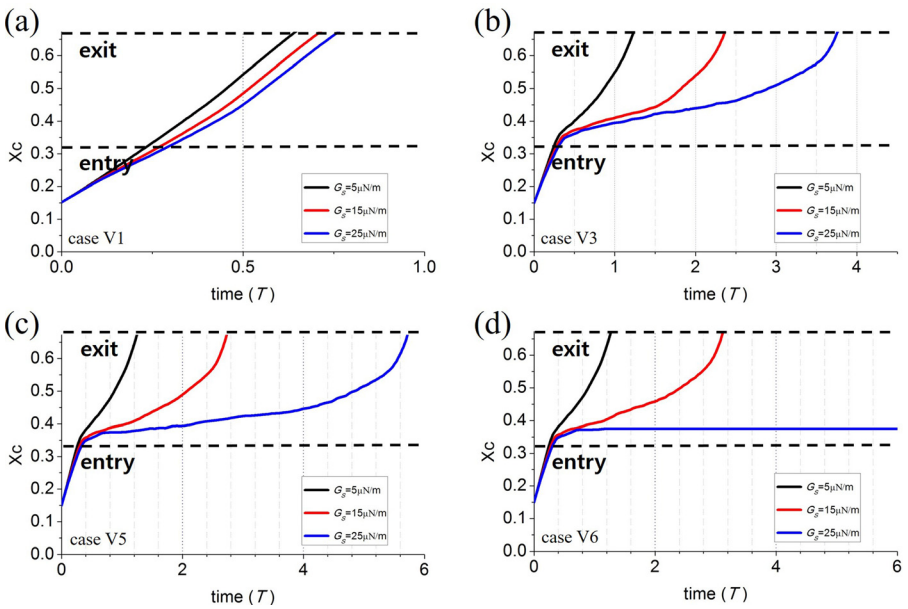


FIG. 6. Trajectories of red blood cells (RBCs) through the narrow channel as a function of the characteristic time for different values of volume stiffness: (a) $k_V = 0.0065$, (b) $k_V = 0.008$, (c) $k_V = 0.0095$, and (d) $k_V = 0.011$.

TABLE I. Cases for effects of volume stiffness.

| | $k_s$ | $k_{AL}$ | $k_{AG}$ | $k_B$ | $k_V$ |
|---|---|---|---|---|---|
| Case V1 | $0.001\,f(G_s)$ | $2\,k_s$ | $0.01\,f(G_s)$ | $0.2\,k_s$ | 0.0 |
| Case V2 | $0.001\,f(G_s)$ | $2\,k_s$ | $0.01\,f(G_s)$ | $0.2\,k_s$ | 0.0050 |
| Case V3 | $0.001\,f(G_s)$ | $2\,k_s$ | $0.01\,f(G_s)$ | $0.2\,k_s$ | 0.0065 |
| Case V4 | $0.001\,f(G_s)$ | $2\,k_s$ | $0.01\,f(G_s)$ | $0.2\,k_s$ | 0.0080 |
| Case V5 | $0.001\,f(G_s)$ | $2\,k_s$ | $0.01\,f(G_s)$ | $0.2\,k_s$ | 0.0095 |
| Case V6 | $0.001\,f(G_s)$ | $2\,k_s$ | $0.01\,f(G_s)$ | $0.2\,k_s$ | 0.0110 |

causes the RBC to become less deformable.[45] According to other studies, malaria-infected RBCs are less deformable than healthy RBCs, and infected RBCs show greater transit time for escaping a narrow channel.[12]

Figure 7 shows velocity of the center of RBCs, $X_c$, as a function of the characteristic time at different values of volume stiffness. The velocity of the center of RBCs was calculated by means of the gradient of $X_c$. Case V1, where $k_V$ is 0, shows different characteristics as compared to other cases. The velocity of $X_c$ decreased with the increase in shear modulus. The cases of high shear modulus revealed low velocity in the narrow channel. When $k_V$ was low, the difference between the shear modulus 5 $\mu$N/m and shear modulus 25 $\mu$N/m was smaller, whereas this difference grows as $k_V$ increases. When the RBC reached the entry of the narrow channel and began to deform, velocity decreased. Nonetheless, the velocity of the RBC did not change during passage through the narrow channel, increasing again when the cell passed the exit. When $X_c$ reached the exit, the velocity of $X_c$ increased independently of the change in $k_V$. An increase in $k_V$ increases both resistance and transit time because it affects the RBC while it is entering the narrow channel.

As shown in Fig. 8, when shear modulus is 5 $\mu$N/m, the transit time for each case is slightly different, but as shear modulus increases, the influence of $k_V$ on transit time increases.

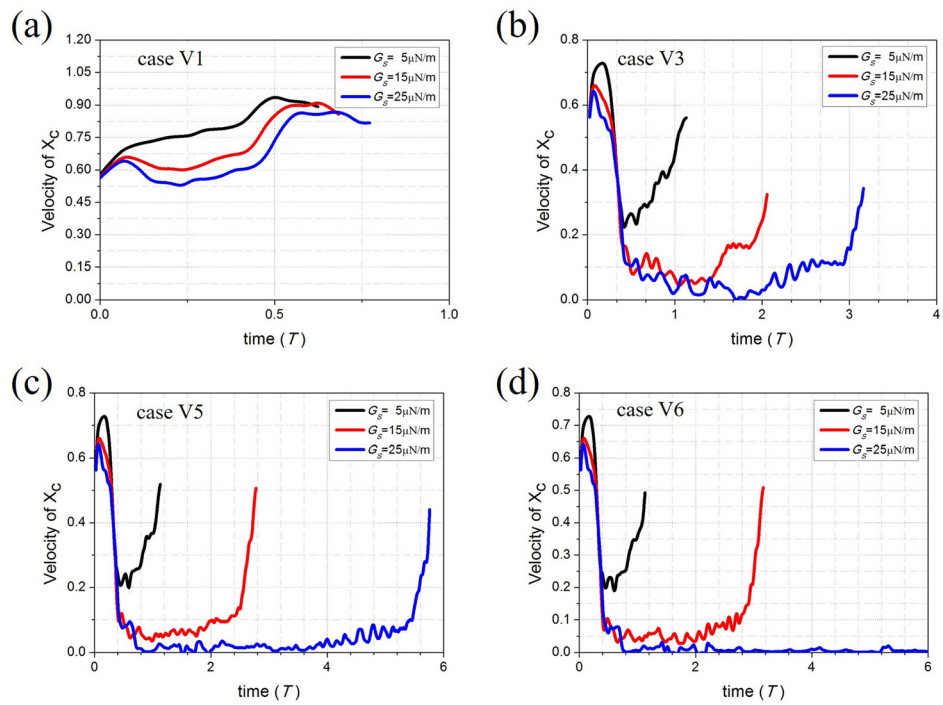


FIG. 7. The velocity of the center of red blood cells (RBCs) as a function of the characteristic time at different values of volume stiffness: (a) $k_V = 0.0$, (b) $k_V = 0.0065$, (c) $k_V = 0.0095$, and (d) $k_V = 0.011$.

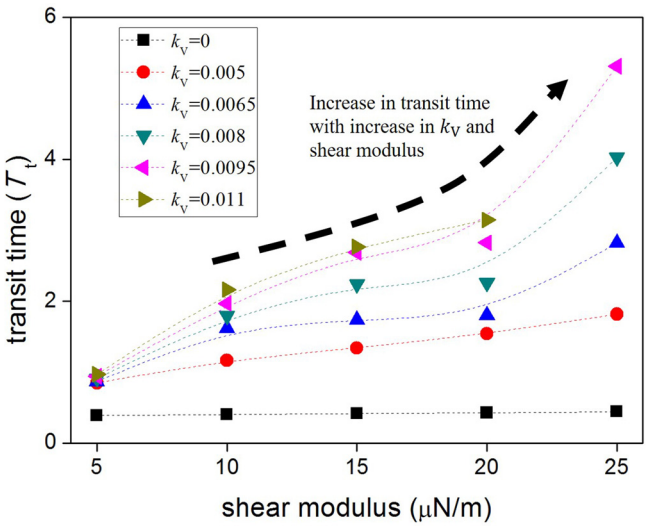


FIG. 8. The effect of the volume stiffness on the transit time of red blood cells (RBCs) from entry to exit as a function of shear modulus.

When $k_V$ is 0, the RBC could not restore its original shape; therefore, the transit time did not change regardless of the increase in shear modulus. When $k_V$ is low ($k_V = 0.005$), the transit time increases linearly with the increase in shear modulus. As $k_V$ increases, however, the relationship between shear modulus and transit time becomes nonlinear. As $k_V$ increases, the transit time also increases; when shear modulus is $25\,\mu\text{N/m}$, shown in case V6, RBC cannot pass through the channel. This result can prove that $k_V$ affects the transit time, which is directly related to RBC rigidity. Therefore, it is important to control $k_V$ in order to determine the rigidity of the RBC.

### Effects of global area stiffness $k_{AG}$

Figure 9 depicts a transit time graph for cases A1–A5. It was shown that when shear modulus is $5\,\mu\text{N/m}$, the transit time for each case is slightly different, but as shear modulus increases, the influence of $k_{AG}$ on transit time increases (Table II). In contrast, when $k_{AG}$ is over

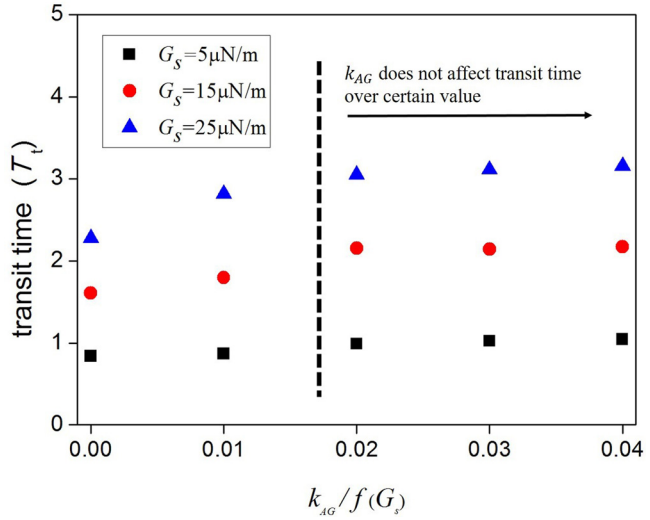


FIG. 9. The effect of the global area stiffness on the transit time of red blood cells (RBCs) from entry to exit as a function of shear modulus.

TABLE II. Cases for effects of global area stiffness.

| | $k_s$ | $k_{AL}$ | $k_{AG}$ | $k_B$ | $k_V$ |
|---|---|---|---|---|---|
| Case A1 | $0.001\,f(G_s)$ | $2\,k_s$ | 0 | $0.2\,k_s$ | 0.0065 |
| Case A2 | $0.001\,f(G_s)$ | $2\,k_s$ | $0.01\,f(G_s)$ | $0.2\,k_s$ | 0.0065 |
| Case A3 | $0.001\,f(G_s)$ | $2\,k_s$ | $0.02\,f(G_s)$ | $0.2\,k_s$ | 0.0065 |
| Case A4 | $0.001\,f(G_s)$ | $2\,k_s$ | $0.03\,f(G_s)$ | $0.2\,k_s$ | 0.0065 |
| Case A5 | $0.001\,f(G_s)$ | $2\,k_s$ | $0.04\,f(G_s)$ | $0.2\,k_s$ | 0.0065 |

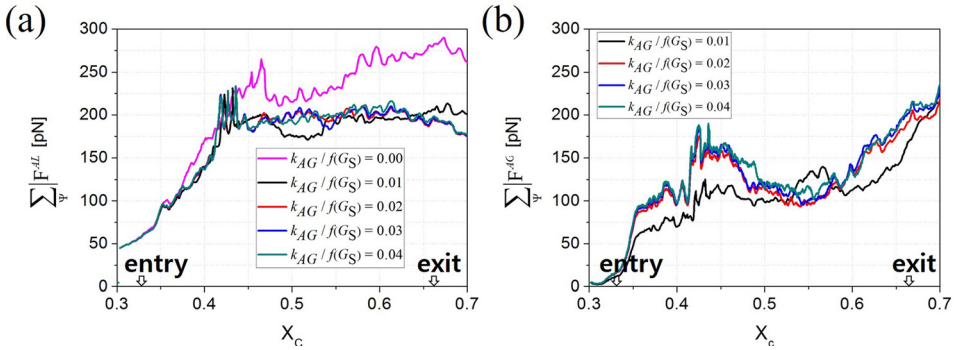


FIG. 10. Total magnitude of the force of (a) local area constraint and (b) global area constraint at $G_s = 25(\mu\text{N/M})$.

0.02, $k_{AG}$ does not affect the transit time. $k_{AG}$ is not a crucial parameter for modeling of the cell because the local area dilation conservation term is present as shown in Eq. (17).

Figure 10 shows the total magnitude of local area constraint force $\sum_\Psi |\mathrm{F}^{AL}|$ and global area constraint force $\sum_\Psi |\mathrm{F}^{AG}|$. The time average of area change during the transit for cases A1-A5 at $G_s = 25(\mu\text{N/M})$ is 4.16%, 1.43%, 0.47%, 0.33%, and 0.26%, respectively. When the RBC entered the narrow channel and began to deform, both total magnitude of local and global area constraint forces increased. There was only the restoring force of the local area dilation, when $k_{AG}$ is 0.0. Therefore, more local area force was needed in order to maintain the area, and it caused the largest change of total area with $k_{AG} = 0.0$. With the increase of $k_{AG}$, $\sum_\Psi |\mathrm{F}^{AG}|$ have increased, while $\sum_\Psi |\mathrm{F}^{AL}|$ have decreased. When $k_{AG}$ is over 0.02 ($k_{AG} > 20\ k_S$), the area change of RBC remains less than 0.5% and transit time reaches a plateau.

## CONCLUSION

In this paper, three major issues related to cell analysis in a microchannel were studied. First, the boundary thickness was analyzed, which is related to the repulsive force critical for the interaction between the cell and wall. When boundary thickness was less than 1.0, unnatural deformation of RBC was observed. As boundary thickness increases, the volume where an RBC could exist decreases; the volume of the fluid does not change. Second, the effect of $k_V$ on transit time in a microchannel was analyzed. As $k_V$ increases, the transit time of the RBC also increases, as if the RBC is infected by a malarial parasite and the rigidity increases. If $k_V$ is nonexistent, the RBC cannot restore its original shape. This result reveals that $k_V$ must be used for proper modeling of the RBC. Third, the $k_{AG}$ value was analyzed, which was proven to not be crucial for modeling of the cell. $k_{AG}$, the parameter representing the total area of RBC, influenced the transit of RBC with 0.5% or bigger change in the total area, whereas there has been slight influence observed when the change in the total area was kept less than 0.5%. The amount of change in the total area was kept less than 0.5% when $k_{AG}$ was 0.02 or bigger.

In summary, the effects of $k_V$ and $k_{AG}$ on cell behavior were studied here. Although the effects of $k_V$ and $k_{AG}$ were proved, a correlation between those and actual cell properties has

not been demonstrated yet. Generally, the volume conservation parameters have been set large enough to maintain the volume. However, from this study, the authors have found out that the volume constant not only maintains the incompressibility of a cell but also influences the characteristics of cells and changes the transition of it. Therefore, volume conservation parameter is related to both incompressibility and rigidity of cells. This study might help to set up the parameters required for the simulation with empirical results. Therefore, it is necessary to determine the correlation between every stiffness variable, and cell properties must be determined in future studies in order to design accurate simulations.

## ACKNOWLEDGMENTS

This work was supported by a grant from the Midcareer Researcher Programs of the National Research Foundation of Korea (NRF), funded by the Ministry of Science, ICT, and Future Planning (Grant No. NRF-2015R1A2A1A15056182). This work was also supported by the National Research Foundation of Korea (NRF) Grant funded by the Korean Government (MSIP) (No. 2015R1A5A1037668).

## APPENDIX: LATTICE UNIT CONVERSION

The conversion of LBM units to *Systéme International* (SI) units starts with fixing the length unit. Generally, LBM uses one lattice for calculating the length unit. When the lattice 100 represents physical domain length 100 $\mu$m ($10^{-4}$ m), the following equation applies:

$$100LL = 10^{-4}\,\mathrm{m} \rightarrow 1LL = 10^{-6}\,\mathrm{m}, \tag{A1}$$

where $LL$ represents the lattice length ($LL$). Therefore, one lattice length represents $10^{-6}$ m in the physical domain. After $LL$ is determined, lattice mass ($LM$) can be determined by fixing the density

$$\rho_{lattice} = 1LM/LL^3, \quad \rho_{physical} = 1000\,\mathrm{kg/m^3}, \tag{A2}$$

$$\rho_{lattice} = \rho_{physical} \rightarrow 1LM/LL^3 = 1000\,\mathrm{kg/m^3}, \tag{A3}$$

$$1LM/(10^{-6}\,\mathrm{m})^3 = 1000\,\mathrm{kg/m^3} \rightarrow 1LM = 10^{-15}\,\mathrm{kg}. \tag{A4}$$

Similarly, lattice time ($LT$) can be determined by fixing the viscosity

$$\nu_{lattice} = \frac{1}{6}LL^2/LT\ (when\ \tau = 1), \quad \nu_{physical} = 10^{-6}\,\mathrm{m^2/s}, \tag{A5}$$

$$\nu_{lattice} = \nu_{physical} \rightarrow \quad \frac{1}{6}LL^2/LT = 10^{-6}\,\mathrm{m^2/s}, \tag{A6}$$

$$\frac{1}{6}(10^{-6}\,\mathrm{m})^2/LT = 10^{-6}\,\mathrm{m^2}/s \rightarrow 1LT = \frac{1}{6}10^{-6}\,\mathrm{s}. \tag{A7}$$

Other physical parameters such as lattice force $LF$ can be derived from the determined lattice unit

$$1F_{lattice} = 1LF = 1(LM)(LL)/(LT)^2 \rightarrow 1\left(10^{-15}\,\mathrm{kg}\right)\left(10^{-6}\,\mathrm{m}\right)/\left(\frac{1}{6}10^{6}\,\mathrm{s}\right)^2 = \frac{1}{36}10^{-9}\left(\mathrm{kg\,m/s^2}\right). \tag{A8}$$

[1]Q. Guo, S. P. Duffy, K. Matthews, X. Deng, A. T. Santoso, E. Islamzada, and H. Ma, "Deformability based sorting of red blood cells improves diagnostic sensitivity for malaria caused by Plasmodium falciparum," Lab Chip **16**, 645–654 (2016).

[2]J. Shaw Bagnall, S. Byun, S. Begum, D. T. Miyamoto, V. C. Hecht, S. Maheswarn, S. L. Stott, M. Toner, R. O. Hynes, and S. R. Manalis, "Deformability of Tumor Cells versus Blood Cells," Sci. Reports **5**, 18542 (2015).
[3]J. Y. Moon, S. Kondaraju, W. Choi, and J. S. Lee, "Lattice Boltzmann-immersed boundary approach for vesicle navigation in microfluidic channel networks," Microfluid. Nanofluid. **17**(6), 1061–1070 (2014).
[4]R. M. Hochmuth, "Micropipette aspiration of living cells," J. Biomech. **33**(1), 15–22 (2000).
[5]J. P. Mills, L. Qie, M. Dao, C. T. Lim, and S. Suresh, "Nonlinear elastic and viscoelastic deformation of the human red blood cell with optical tweezers," Mech. Chem. Biosyst.: MCB **1**, 169–180 (2004).
[6]M. J. Rosenbluth, W. A. Lam, and D. A. Fletcher, "Force microscopy of nonadherent cells: A comparison of leukemia cell deformability," Biophys. J. ***90***(8), 2994–3003 (2006).
[7]A. Adamo, A. Sharei, L. Adamo, B. Lee, S. Mao, and K. F. Jensen, "Microfluidics-based assessment of cell deformability," Anal. Chem. **84**(15), 6438–6443 (2012).
[8]P. Preira, V. Grandne, J. M. Forel, S. Gabriele, M. Camara, and O. Theodoly, "Passive circulating cell sorting by deformability using a microfluidic gradual filter," Lab Chip **13**(1), 161–170 (2013).
[9]H.-S. Moon *et al*., "Continuous separation of breast cancer cells from blood samples using multi-orifice flow fractionation (MOFF) and dielectrophoresis (DEP)," Lab Chip **11**(6), 1118–1125 (2011).
[10]D. R. Gossett, T. K. Henry, S. A. Lee, Y. Ying, A. G. Lindgren, O. O. Yang, J. Rao, A. T. Clark, and D. Di Carlo, "Hydrodynamic stretching of single cells for large population mechanical phenotyping," Proc. Natl. Acad. Sci., **109**(20), 7630–7635 (2012).
[11]O. Otto, P. Rosendahl, A. Mietke, S. Golfier, C. Herold, D. Klaue, and M. Wobus, "Real-time deformability cytometry: On-the-fly cell mechanical phenotyping," Nature Methods **12**(3), 199–202 (2015).
[12]T. Wu and J. J. Feng, "Simulation of malaria-infected red blood cells in microfluidic channels: Passage and blockage," Biomicrofluidics **7**(4), 044115 (2013).
[13]T. Wu, Q. Guo, H. Ma, and J. J. Feng, "The critical pressure for driving a red blood cell through a contracting microfluidic channel," Theor. Appl. Mech. Lett. **5**(6), 227–230 (2015).
[14]D. A. Fedosov, H. Noguchi, and G. Gompper, "Multiscale modeling of blood flow: From single cells to blood rheology," Biomech. Model. Mechanobiol. **13**(2), 239–258 (2014).
[15]H. Noguchi and G. Gompper, "Shape transitions of fluid vesicles and red blood cells in capillary flows," Proc. Natl. Acad. Sci. U. S. A. **102**(40), 14159–14164 (2005).
[16]M. M. Dupin, I. Halliday, C. M. Care, L. Alboul, and L. L. Munn, "Modeling the flow of dense suspensions of deformable particles in three dimensions," Phys. Rev. E **75**(6), 066707 (2007).
[17]Y. Imai, H. Kondo, T. Ishikawa, C. T. Lim, and T. Yamaguchi, "Modeling of hemodynamics arising from malaria infection," J. Biomech. **43**(7), 1386–1393 (2010).
[18]T. Ye, N. Phan-Thien, B. C. Khoo, and C. T. Lim, "Dissipative particle dynamics simulations of deformation and aggregation of healthy and diseased red blood cells in a tube flow," Phys. Fluids (1994-present) **26**(11), 111902 (2014).
[19]J. B. Freund, "Numerical simulation of flowing blood cells," Annu. Rev. Fluid Mech. **46**, 67–95 (2014);
[20]M. Nakamura, S. Bessho, and S. Wada, "Spring-network-based model of a red blood cell for simulating mesoscopic blood flow," Int. J. Numer. Methods Biomed. Eng. **29**(1), 114–128 (2013).
[21]I. Jancigova and T. Renata, "Scalability of forces in mesh-based models of elastic objects," in ELEKTRO (IEEE, 2014).
[22]G. Gompper and D. M. Kroll, "Network models of fluid, hexatic and polymerized membranes," J. Phys.: Condens. Matter **9**(42), 8795 (1997).
[23]E. A. Evans, R. Skalak, and S. Weinbaum, "Mechanics and thermodynamics of biomembranes" (CRC Press, Boca Raton, 1980).
[24]D. A. Fedosov, "Multiscale modeling of blood flow and soft matter," Doctoral dissertation (Brown University, 2010)).
[25]T. Krüger, B. Kaoui, and J. Harting, "Interplay of inertia and deformability on rheological properties of a suspension of capsules," J. Fluid Mech. **751**, 725–745 (2014).
[26]J. Dupire, M. Socol, and A. Viallat, "Full dynamics of a red blood cell in shear flow," Proc. Natl. Acad. Sci. **109**(51), 20808–20813 (2012).
[27]M. Abkarian and A. Viallat, "Vesicles and red blood cells in shear flow," Soft Matter **4**(4), 653–657 (2008).
[28]J. S. Lee, J. Y. Moon, and J. S. Lee, "Study of transporting of droplets on heterogeneous surface structure using the lattice Boltzmann approach," Appl. Thermal Eng. **72**(1), 104–113 (2014).
[29]H. Farhat, S. Kondaraju, and J. S. Lee, *Accelerated Lattice Boltzmann Model for Colloidal Suspensions* (Springer, 2014).
[30]Y. W. Kim, J. Y. Moon, K. R. Cho, and J. S. Lee, "Impedance boundary condition analysis of aging-induced wave reflections in blood flow," Korea-Austr. Rheol. J. **25**(4), 217–225 (2013).
[31]Z. Guo, C. Zheng, and B. Shi, "Discrete lattice effects on the forcing term in the lattice Boltzmann method," Phys. Rev. E **65**(4), 046308 (2002).
[32]I. Jančigová and I. Cimrák, "Non-uniform force allocation for area preservation in spring network models," Int. J. Numer. Methods Biomed. Eng. e02757 (2015).
[33]D. A. Fedosov, B. Caswell, and G. E. Karniadakis, "A multiscale red blood cell model with accurate mechanics, rheology, and dynamics," Biophys. J. **98**(10), 2215–2225 (2010).
[34]H. S. Seung and D. R. Nelson, "Defects in flexible membranes with crystalline order," Phys. Rev. A **38**(2), 1005 (1988).
[35]X. Shi, G. Lin, J. Zou, and D. A. Fedosov, "A lattice Boltzmann fictitious domain method for modeling red blood cell deformation and multiple-cell hydrodynamic interactions in flow," Int. J. Numer. Methods Fluids **72**(8), 895–911 (2013).
[36]D. A. Reasor, J. R. Clausen, and C. K. Aidun, "Coupling the lattice-Boltzmann and spectrin-link methods for the direct numerical simulation of cellular blood flow," Int. J. Numer. Methods Fluids **68**(6), 767–781 (2012).
[37]C. S. Peskin, "The immersed boundary method," Acta Numerica **11**, 479–517 (2002).
[38]C. Pozrikidis, "Effect of membrane bending stiffness on the deformation of capsules in simple shear flow," J. Fluid Mech. **440**, 269–291 (2001).
[39]Z. G. Feng and E. E. Michaelides, "The immersed boundary-lattice Boltzmann method for solving fluid–particles interaction problems," J. Comput. Phys. **195**(2), 602–628 (2004).
[40]E. Evans and Y. C. Fung, "Improved measurements of the erythrocyte geometry," Microvasc. Res. **4**(4), 335–347 (1972).

[41]S. M. McFaul, B. K. Lin, and H. Ma, "Cell separation based on size and deformability using microfluidic funnel ratchets," Lab Chip **12**(13), 2369–2376 (2012).
[42]D. J. Quinn, I. Pivkin, S. Y. Wong, K. H. Chiam, M. Dao, G. E. Karniadakis, and S. Suresh, "Combined simulation and experimental study of large deformation of red blood cells in microfluidic systems," Ann. Biomed. Eng. **39**(3), 1041–1050 (2011).
[43]C. Dong and R. Skalak, "Leukocyte deformability: finite element modeling of large viscoelastic deformation," J. Theor. Biol. **158**(2), 173–193 (1992).
[44]A. Taloni, E. Kardash, O. U. Salman, L. Truskinovsky, S. Zapperi, and C. A. La Porta, "Volume changes during active shape fluctuations in cells," Phys. Rev. Lett. **114**(20), 208101 (2015).
[45]A. G. Maier, B. M. Cooke, A. F. Cowman, and L. Tilley, "Malaria parasite proteins that remodel the host erythrocyte," Nat. Rev. Microbiol. **7**(5), 341–354 (2009).